Research Square

Preprints are preliminary reports that have not undergone peer review.
They should not be considered conclusive, used to inform clinical practice,
or referenced by the media as validated information.

Quantum Criticality Correlations in a Transverse-Field Anisotropic Cluster-XX Chain

Mohammad Abbasi
University of Guilan
Nima Mahboob
University of Guilan
Saeed Mahdavifar
smahdavifar@gmail.com
University of Guilan

Article

Keywords:

Posted Date: November 3rd, 2026

DOI: https://doi.org/10.21203/rs.3.rs-11233788/v1

License: This work is licensed under a Creative Commons Attribution 4.0 International License.
Read Full License

Additional Declarations: No competing interests reported.

Quantum Criticality Correlations in a Transverse-Field Anisotropic Cluster-XX Chain

M. Abbasi[1], **N. Mahboob**[1], **and S. Mahdavifar**[*1]

[1]Department of Physics, University of Guilan, 41335-1914, Rasht, Iran
[*]smahdavifar@gmail.com

ABSTRACT

We investigate the spin-$1/2$ XX chain with an anisotropic three-spin interaction in a transverse magnetic field, a model in which cluster interactions provide a tunable route to unconventional quantum phases and low-energy spectral reconstructions. We focus on how the anisotropy of the three-spin coupling modifies the field-driven evolution of gapless phases and their quantum correlations beyond the conventional gap-closing scenario. We find a rich phase structure containing both gapped and gapless regimes, including a Lifshitz-type gapless–gapless transition associated with a reconstruction of the low-energy Fermi points while the excitation gap remains closed. For $\beta < 0$, the field can drive a sequence of two gapless phases followed by a gapped phase, whereas for $\beta > 0$ the system is gapless at zero field, becomes gapped immediately upon applying a finite field, and undergoes a further transition at $h = 1$ between distinct gapped regimes. The anisotropy also produces distinct chiral and chiral-nematic correlation patterns, while concurrence and quantum discord reveal qualitatively different distributions of bipartite entanglement and more general nonclassical correlations across the phase diagram. These results show that anisotropic three-spin interactions provide a distinct extension of previously studied cluster-XX chains, in which external fields can reorganize the topology of gapless excitations and the associated correlation structure. The model therefore offers an exactly solvable framework for studying unconventional quantum criticality arising from the interplay of cluster interactions, field control, and quantum correlations.

1 Introduction

Quantum phase transitions (QPTs) arise at zero temperature when nonthermal control parameters drive qualitative changes in the ground state of many-body systems, providing a probe of quantum fluctuations, collective behavior, and ground-state correlations[1–8]. Their phase diagrams characterize competing quantum orders and critical boundaries, with relevance to low-dimensional quantum systems, magnetism, superconductivity, topological order[7,13,14], and quantum information[15–18].

Spin-1/2 chains provide an ideal setting for investigating quantum phase transitions, as they capture the essential physics of strongly correlated systems and can be solved exactly using both analytical and numerical methods[9]. Their reduced dimensionality enhances quantum fluctuations, which can lead to critical behavior and emergent quantum orders that have no classical counterparts in higher dimensions. Within this context, the XX and XY Heisenberg-type models have been widely used to study the interplay between exchange anisotropy, external fields, and many-body correlations[19–24]. These models not only capture both gapless and gapped excitations but also reveal deep connections between quantum magnetism, critical phenomena, and topological phases of matter[25–29]. Moreover, advances in experimental quantum simulation, using ultracold atoms[15], trapped ions[30,31], and superconducting qubit arrays[30], have enabled the precise realization and control of spin-chain Hamiltonians, thereby making these systems important platforms for probing quantum criticality, coherence, and entanglement in low-dimensional quantum materials.

Recent theoretical efforts have shown that extending conventional two-spin exchange models to include cluster spin interactions introduces additional competing energy scales that qualitatively reshape the phase structure of low-dimensional systems. In particular, three-spin interactions (TSI) arise naturally as higher-order exchange processes in platforms such as Mott insulators[32,33], optical lattices[33–35], and superconducting qubit networks[36], and are known to promote frustration, chirality, and nontrivial correlation patterns even in one dimension[25–29,37–46]. These interactions can stabilize phases that are not accessible within conventional two-spin exchange models and give rise to unconventional critical behavior, including transitions that are not accompanied by gap closing.

A particularly distinctive feature of three-spin interactions in one-dimensional spin chains is their ability to generate transitions between distinct gapless phases[37]. In such gapless–gapless transitions, the excitation spectrum remains gapless on both sides of the critical point, while the structure of the low-energy excitations and the topology of the Fermi surface can change qualitatively. This behavior is especially relevant to the present model, where the competition between the conventional XX exchange, anisotropic three-spin interaction, and transverse magnetic field can produce different gapless regimes as well

as field-induced gapped phases. Thus, the anisotropy of the three-spin interaction is not merely an additional coupling, but provides a mechanism for restructuring the low-energy spectrum and modifying the nature of quantum correlations beyond conventional gap-closing transitions.

At the same time, experimental progress has made such models increasingly relevant. Effective three-spin interactions have been engineered in trapped-ion systems, superconducting circuits, and programmable optical lattices, where cluster spin interactions can be tuned with a high degree of control[47–49]. These advances establish TSI models as useful platforms for exploring quantum criticality, frustration, and entanglement in strongly correlated systems.

The possibility of engineering such interactions also motivates the study of their response to external control parameters. In particular, a transverse magnetic field provides a direct and experimentally relevant means of tuning the competition between two-spin exchange and three-spin correlations. Previous studies of related three-spin XX chains have explored field-dependent thermodynamic properties, quantum correlations, and critical behavior[37,50–57]. These studies establish the physical relevance of field-tunable three-spin systems, while also motivating a systematic investigation of how anisotropy in the three-spin coupling modifies their ground-state structure and quantum critical behavior.

In a recent study, the one-dimensional Heisenberg XX chain with anisotropic three-spin interactions (ATSI) in the absence of an external magnetic field was investigated, revealing distinct quantum phases and critical behavior arising from the competition between conventional two-spin exchange and three-spin couplings[46]. Three-spin interactions can give rise to transitions between distinct gapless phases, in which the excitation spectrum remains gapless while the structure of the low-energy excitations changes qualitatively[37]. The response of such unconventional gapless phases to an external magnetic field is therefore of particular interest, as the field can alter their stability, transform the low-energy excitation structure, and drive transitions into gapped phases. Moreover, special cases of three-spin interactions are known to support distinct gapless spin-liquid phases separated by unconventional critical points, whose evolution under a magnetic field can involve successive transitions between different gapless and gapped phases[37,56]. These observations motivate an investigation of how the anisotropy of the three-spin interaction modifies the field-induced evolution of gapless phases and the associated quantum critical behavior.

The transverse magnetic field provides a natural control parameter for probing how the competition between the XX exchange and anisotropic three-spin interaction reshapes the ground-state structure. In this context, quantum correlations provide complementary information on the phases and critical boundaries beyond conventional spectral and order-parameter diagnostics. We therefore analyze bipartite entanglement through concurrence and more general nonclassical correlations through quantum discord, with the aim of determining how these quantities respond to the distinct gapless and gapped regimes generated by the anisotropic interaction.

The remainder of this paper is organized as follows. In Sec. 2, we introduce the model and outline the fermionization approach used to obtain its exact ground state. Section 3 is devoted to the analysis of the resulting energy spectrum, ground-state properties, and quantum phase transitions in the presence of the transverse field. Finally, Sec. 4 summarizes our main conclusions and discusses possible implications of these results for future studies of low-dimensional quantum systems.

2 Model and Energy spectrum

The Hamiltonian of the one-dimensional spin-1/2 XX chain with an ATSI in the presence of a uniform transverse magnetic field is given by

$$\mathscr{H} = J\sum_{n=1}^{N}\left[S_n^xS_{n+1}^x+S_n^yS_{n+1}^y\right]+J'\sum_{n=1}^{N}\left[\left(S_n^xS_{n+2}^y+\beta S_n^yS_{n+2}^x\right)S_{n+1}^z\right]-Jh\sum_{n=1}^{N}S_n^z, \tag{1}$$

where S_n is the spin operator at the n-th site, $J>0$ denotes the antiferromagnetic exchange coupling, J' along with h represent the strengths of the three-spin interaction and the uniform transverse magnetic field, respectively, and N is the system size (i.e., the total number of spins). Periodic boundary conditions $S_{n+N}^{\mu}=S_n^{\mu}$ $(\mu=x,y,z)$ are assumed. Throughout this work, we measure energies in units of J, i.e., we rescale the Hamiltonian as $\mathscr{H}/J$. Accordingly, the dimensionless parameter $\alpha=J'/J$ is introduced, and all energies, including the transverse magnetic field h, are expressed in units of J.

Periodic boundary conditions $S_{n+N}^{\mu}=S_n^{\mu}$ $(\mu=x,y,z)$ are assumed. Here, the dimensionless parameter $\alpha=J'/J$ is defined without loss of generality.

Figure 1 illustrates the ground-state phase diagram of the model defined in Eq. (1) in the absence of the transverse magnetic field. In this zero-field limit, the system remains gapless throughout the parameter space. Moreover, the Lifshitz critical line, defined by $\beta=-\frac{1}{\alpha^2}$, appears for $\alpha\neq 0$ as the boundary separating two distinct gapless regions, thereby marking a gapless-gapless (Lifshitz) quantum phase transition.

To investigate the ground-state properties in presence of a uniform magnetic field, the Hamiltonian in Eq. (1) is diagonalized exactly using the fermionization technique. This is achieved through the Jordan-Wigner transformation, which maps spin

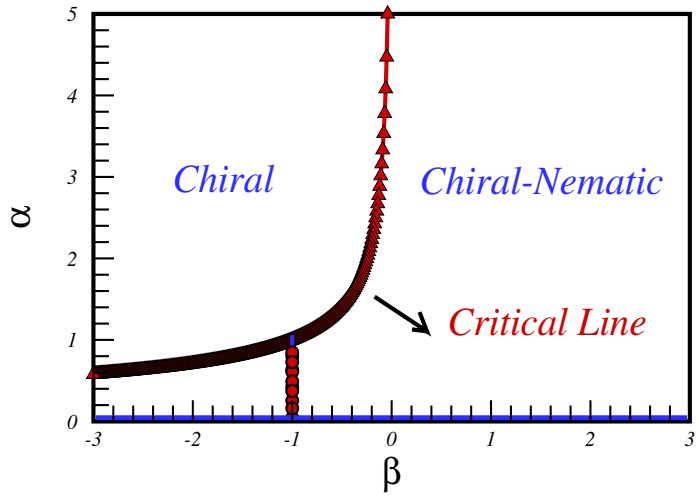


Figure 1. (color online). The ground state phase diagram in the β-α plane. At $\alpha = 0$, where the system reduces to the pure spin-1/2 XX chain, the ground state resides in the Luttinger liquid phase. Similarly, when $\beta = -1$ and $\alpha < 1$, the ground state remains in the Luttinger liquid phase[46].

operators onto spinless fermionic operators as follows:

$$\begin{aligned} S_n^+ &= a_n^\dagger e^{i\pi(\Sigma_{l<n} a_l^\dagger a_l)}, \\ S_n^- &= a_n e^{i\pi(\Sigma_{l<n} a_l^\dagger a_l)}, \\ S_n^z &= a_n^\dagger a_n - \frac{1}{2}, \end{aligned} \tag{2}$$

where $a_n^\dagger$ and a_n denote the fermionic creation and annihilation operators, respectively. Under this transformation, the Hamiltonian takes a quadratic form in terms of fermionic operators:

$$\begin{aligned} \mathscr{H}/J &= \frac{1}{2}\sum_{n=1}^{N}\left(a_n^\dagger a_{n+1} + a_{n+1}^\dagger a_n\right) + \frac{i}{8}\alpha(\beta-1)\sum_{n=1}^{N}\left(a_n^\dagger a_{n+2} - a_{n+2}^\dagger a_n\right) \\ &+ \frac{i}{8}\alpha(\beta+1)\sum_{n=1}^{N}\left(a_n^\dagger a_{n+2}^\dagger - a_{n+2} a_n\right) - h\sum_{n=1}^{N}\left(a_n^\dagger a_n - \frac{1}{2}\right). \end{aligned} \tag{3}$$

By performing a Fourier transformation, $a_n = \frac{1}{\sqrt{N}}\sum_k e^{-ikn} a_k$, followed by a Bogoliubov transformation:

$$a_k = \cos(\theta_k)\gamma_k - \sin(\theta_k)\gamma_{-k}^\dagger, \tag{4}$$

the Hamiltonian can thus be diagonalized and expressed in the following form:

$$\mathscr{H}/J = \sum_{k=-\pi}^{\pi} \varepsilon(k)(\gamma_k^\dagger \gamma_k - \frac{1}{2}). \tag{5}$$

with energy spectrum

$$\varepsilon(k) = \sqrt{\mathscr{A}_k^2 + \mathscr{C}_k^2} + \mathscr{B}_k, \tag{6}$$

where,

$$\begin{aligned} \mathscr{A}_k &= \cos(k) - h, \\ \mathscr{B}_k &= \frac{1}{4}\alpha(\beta-1)\sin(2k), \\ \mathscr{C}_k &= \frac{1}{4}\alpha(\beta+1)\sin(2k), \\ \tan(2\theta_k) &= \frac{\mathscr{C}_k}{\mathscr{A}_k}. \end{aligned} \tag{7}$$

The summation in Eq. (5) is performed over discrete momentum values $k = 2\pi m/N$, where $m = 0, \pm 1, \ldots, \pm(N-1)/2$ for odd N, and $m = 0, \pm 1, \ldots, \pm(N/2-1), N/2$ for even N, under the assumption of periodic boundary conditions for the Jordan-Wigner fermions. In the thermodynamic limit $N \to \infty$, the ground state of the system is obtained by filling all single-particle states with $\varepsilon(k) \leq 0$ and leaving those with $\varepsilon(k) > 0$ unoccupied.

From the structure of the fermionic spectrum, we identify four distinct critical lines that govern the phase diagram of the model. In the region $\beta < 0$, the system exhibits two field-driven critical points given by

$$h_{c_1} = \sqrt{1-p_+^2}\,(qp_+ - 1), \qquad \beta < -\frac{1}{\alpha^2}, \tag{8}$$

$$h_{c_2} = \sqrt{1-p_-^2}\,(q|p_-| + 1), \qquad \beta < 0, \qquad h_{c_2} > 1. \tag{9}$$

where

$$p_\pm = \frac{1 \pm \sqrt{1+8q^2}}{4q}, \qquad q = |\alpha|\sqrt{|\beta|}. \tag{10}$$

We will show that the first critical field, h_{c_1}, corresponds to a gapless–gapless transition of Lifshitz type, associated with a change in the topology of the Fermi surface without opening of a gap in the excitation spectrum. This critical line exists for $\beta < -1/\alpha^2$, where it emerges from the corresponding zero-field Lifshitz critical point. The second critical field, h_{c_2}, marks a conventional gapless–gapped transition, where a finite energy gap develops in the excitation spectrum. For $\beta < 0$, this critical line occurs in the regime $h_{c_2} > 1$. These two transitions delimit an intermediate regime characterized by a distinct gapless phase with a modified low-energy excitation structure.

For $\beta > 0$, the system exhibits two critical boundaries in the field direction, located at

$$h_c^{(0)} = 0, \qquad h_c^{(1)} = 1. \tag{11}$$

At zero field, the system remains gapless for $\beta > 0$, consistent with the gapless phase of the zero-field model. Upon applying an infinitesimal transverse field, a finite excitation gap opens immediately, so that $h = 0$ represents a gapless–gapped critical boundary. As the field is further increased, the system undergoes a second transition at $h_c^{(1)} = 1$, where the excitation gap closes and subsequently reopens. This field-driven transition is independent of the anisotropy strength within the $\beta > 0$ regime and separates two distinct gapped phases. In addition to the field-driven transitions, the system exhibits an interaction-driven critical line at

$$\beta_c = 0, \tag{12}$$

for $h < 1$. This transition separates the $\beta < 0$ and $\beta > 0$ regions and corresponds to a qualitative change in the ground-state structure, distinguishing distinct phases with different correlation properties across the anisotropy-driven boundary.

Together, these critical lines define the global phase diagram and reflect the interplay between the transverse magnetic field and the ATSI in determining the nature of the quantum phases and their associated critical behavior.

3 Results

3.1 Phase transition in the ground state

We begin our analysis by focusing on the ground-state energy density, which captures the stability and collective behavior of the many-body ground state and serves as a central quantity for identifying quantum phase transitions. Throughout this work, we fix the energy scale by setting $J = 1$ and consider a system size $N = 1000$, which provides a reliable approximation to the thermodynamic limit.

Within the fermionic representation, the ground-state energy density is obtained by summing over the occupied and unoccupied single-particle modes and can be written as

$$E_G = \frac{1}{2N}\sum_{k\in\Lambda}\varepsilon(k) - \frac{1}{2N}\sum_{k\notin\Lambda}\varepsilon(k), \tag{13}$$

where $\varepsilon(k)$ denotes the fermionic dispersion relation and Λ represents the set of momentum modes occupied in the ground state. This expression reflects the filling structure of the fermionic spectrum and shows how the ground-state energy is determined by the competition between occupied and unoccupied quasiparticle states.

The behavior of E_G as a function of the model parameters provides direct insight into the underlying quantum phases. Nonanalytic features in the ground-state energy or its derivatives signal quantum phase transitions, and mark qualitative changes

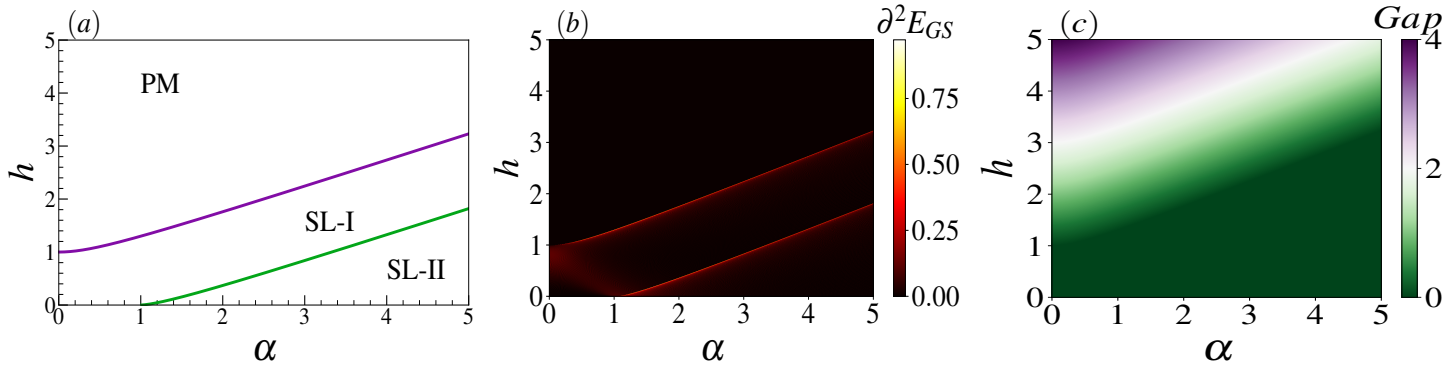


Figure 2. (color online). (a) Schematic ground-state phase diagram in the (α, h) parameter space for fixed $\beta = -1$. (b) Density plot of the second derivative of the ground-state energy in the (α, h) plane. (c) Density plot of the energy gap in the (α, h) parameter space. All results are obtained for a chain of size $N = 1000$.

in the structure of the many-body ground state. In particular, variations in the dispersion relation that change the location or number of Fermi points can lead to distinct quantum phases and different types of critical behavior.

Closely related to the ground-state energy is the excitation gap, defined as the minimum energy required to create a quasiparticle excitation above the ground state. In the present fermionic representation, this quantity is determined by the structure of the single-particle spectrum and, in particular, by the behavior of the dispersion relation near the Fermi level. A vanishing gap indicates the presence of gapless excitations and is typically associated with critical or quantum liquid phases, whereas a finite gap signals a stable phase with suppressed low-energy fluctuations. Consequently, the evolution of the ground-state energy, together with the opening or closing of the energy gap, offers a comprehensive framework for identifying quantum critical points and characterizing the emergent quantum phases of the system.

Before discussing the phase diagram for the general anisotropic case, it is useful to consider the special limit $\beta = -1$, which corresponds to a previously studied limit of the three-spin-interaction XX chain[37,52]. This limit provides a useful reference point because its zero-field phase diagram contains two distinct gapless spin-liquid phases, denoted by SL-I and SL-II, separated by a quantum critical point at $\alpha = 1$. In the presence of a transverse magnetic field, an additional paramagnetic (PM) phase emerges, leading to a particularly transparent realization of field-driven quantum phase transitions. For $\beta = -1$, the two relevant critical fields can be written as

$$h_{c_1}^{sp}(\alpha) = \sqrt{1 - s_+^2}\,(\alpha s_+ - 1), \qquad \alpha > 1, \tag{14}$$

$$h_{c_2}^{sp}(\alpha) = \sqrt{1 - s_-^2}\,(1 - \alpha s_-), \qquad \alpha > 0, \tag{15}$$

where

$$s_\pm = \frac{1 \pm \sqrt{1 + 8\alpha^2}}{4\alpha}. \tag{16}$$

The first critical line $h_{c_1}^{sp}$ exists for $\alpha > 1$ and separates the SL-II and SL-I phases. The second critical line h_{c_2} exists for $\alpha > 0$ and separates the gapless spin-liquid regime from the gapped paramagnetic phase. Thus, for $\alpha > 1$, increasing the magnetic field drives the system successively from SL-II to SL-I and then to the PM phase, whereas for $0 < \alpha < 1$ the zero-field state belongs to the SL-I phase and the system undergoes a direct transition from SL-I to PM at $h_{c_2}^{sp}$.

Figure 2(a) shows the resulting schematic phase diagram in the α–h plane for $\beta = -1$, that the three phases SL-II, SL-I, and PM and the corresponding critical boundaries h_{c_1} and h_{c_2}. The corresponding singular behavior of the second derivative of the ground-state energy, shown in Fig. 2(b), identifies the two critical boundaries, while the energy gap density plot in Fig. 2(c) demonstrates the opening of a finite gap upon crossing the h_{c_2} boundary into the PM phase.

The special case $\beta = -1$ also motivates our choice of $\alpha = 2$ for the main analysis. We choose $\alpha = 2$ because it lies in the $\alpha > 1$ regime, where the reference phase diagram contains all three relevant phases, SL-II, SL-I, and PM, and therefore provides a convenient representative parameter choice for investigating how the anisotropy parameter β modifies the quantum phases and critical behavior. This choice allows us to study the effect of β across the different regimes of the model while avoiding the additional zero-field structure associated with the $\alpha < 1$ regime, including the additional Luttinger-liquid region and the triple point at $\beta = -1$.

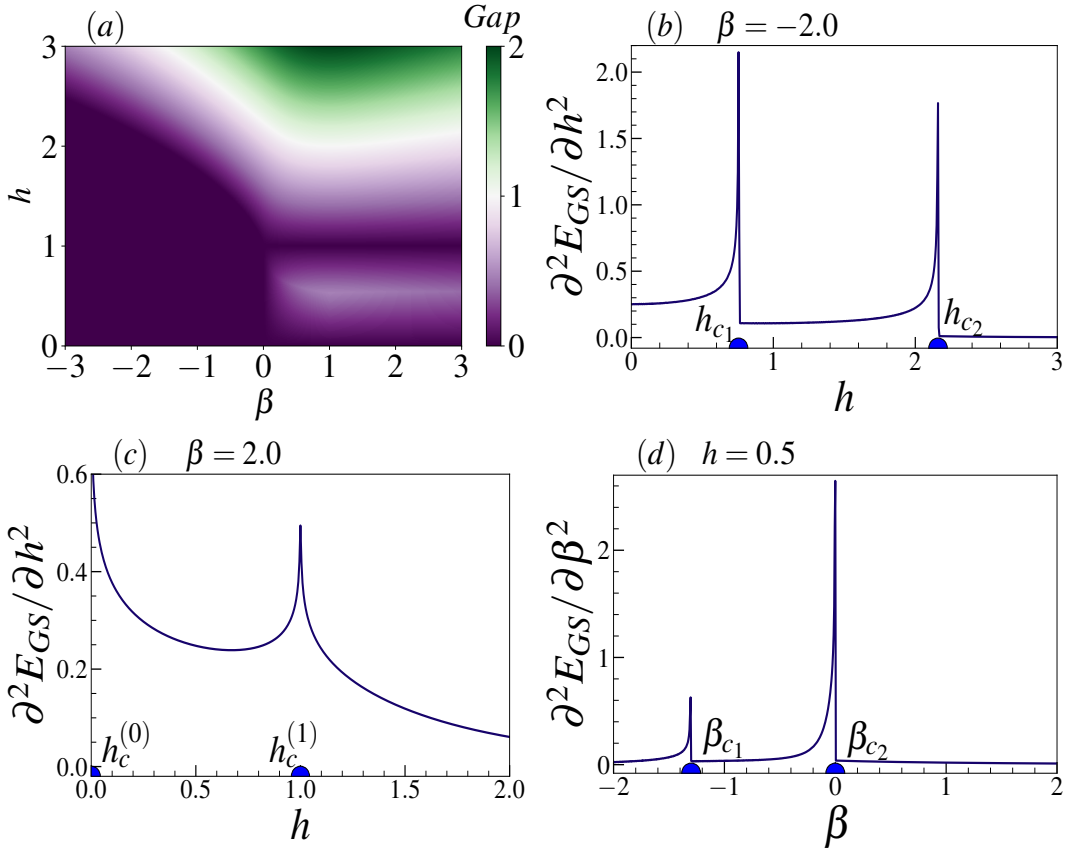


Figure 3. (color online). (a) Presents the density plot of the energy gap as a function of the transverse magnetic field h and the anisotropy parameter β. (b) and (c) Show the second derivative of the ground-state energy with respect to the magnetic field for fixed anisotropy values $\beta = -2.0$ and $\beta = 2.0$, respectively. (d) Displays the second derivative of the ground-state energy with respect to β at a fixed $h = 0.5$. All results are obtained for a chain of size $N = 1000$, and $\alpha = 2.0$.

Figure 3 (a) shows the density plot of the energy gap as a function of the anisotropy parameter β and the transverse magnetic field h. Three distinct regions are clearly identified in the phase space, consisting of one gapless phase and two gapped phases. These regions are separated by three well-defined critical lines, which signal quantum phase transitions driven by changes in the external magnetic field and interaction anisotropy.

In particular, one critical line occurs at $\beta_c = 0.0$ for field strengths $h \leq 1$, indicating a transition associated with the anisotropy of the three-spin interaction. For $\beta > 0.0$, two critical boundaries are present at $h_c^{(0)} = 0$ and $h_c^{(1)} = 1$. The boundary at $h_c^{(0)} = 0$ separates the gapless zero-field state from the gapped phase that emerges immediately upon applying a finite transverse field, while the boundary at $h_c^{(1)} = 1$ corresponds to a field-driven transition associated with the closing and reopening of the excitation gap. The third critical boundary, denoted by $h_c(\beta)$, appears in the region $\beta < 0.0$, where the combined effects of anisotropy and the transverse field give rise to the opening of a finite energy gap.

The closing of the gap along these critical lines signals qualitative changes in the low-energy excitation spectrum, marking the boundaries between distinct quantum phases. The resulting phase diagram highlights the rich interplay between the anisotropic three-spin interaction and the transverse magnetic field, and underscores the role of cluster spin interactions in shaping the quantum critical behavior of the system.

To further characterize the nature of the phase transitions identified from the excitation gap, we analyze the second derivative of the ground-state energy, which serves as a sensitive probe of quantum criticality, particularly in cases where gap-based diagnostics alone may be inconclusive. Nonanalytic behavior or discontinuities in higher-order derivatives of the ground-state energy are well-established signatures of continuous quantum phase transitions.

Figure 3 (b) presents the second derivative of the ground-state energy with respect to the transverse magnetic field, $\partial^2 E_G/\partial h^2$, for fixed parameters $\alpha = 2.0$ and $\beta = -2.0$. As seen in Fig. 3 (a), this parameter regime exhibits a transition from a gapless phase to a gapped phase as the field is increased. Consistent with this picture, two clear discontinuities are observed

in Fig. 3 (b). The first critical point, denoted by h_{c_1}, signals a transition between two distinct gapless phases, which is not accompanied by the opening of an energy gap and therefore cannot be detected from the gap analysis alone. The second critical point, h_{c_2}, corresponds to the transition from the gapless phase to a gapped phase, in agreement with the closing and reopening of the energy gap observed in Fig. 3 (a). This shows that the ground-state energy captures additional critical information beyond that provided by the excitation spectrum.

In Fig. 3 (c), we show $\partial^2 E_G/\partial h^2$ for $\alpha = 2.0$ and $\beta = 2.0$. In this case, a single sharp peak appears at $h_c^{(1)} = 1.0$, signaling a continuous quantum phase transition. This critical point coincides with the gap-closing line identified in the energy-gap density plot, confirming that the transition is of second order and arises from field-induced changes in the low-energy excitation structure.

Figure 3 (d) presents the second derivative of the ground-state energy with respect to the anisotropy parameter, $\partial^2 E_G/\partial \beta^2$, for fixed $\alpha = 2.0$ and $h = 0.5$. For $\beta < 0$, the system lies in a gapless region, where a clear nonanalytic feature signals a transition between distinct gapless phases. As β increases, a sharp discontinuity emerges at $\beta_c = 0$, marking the transition from a gapless phase to a gapped phase. This critical behavior is consistent with the phase boundaries extracted from the energy gap, further confirming a second-order quantum phase transition.

Taken together, these results demonstrate that while the energy gap reliably identifies gapped-gapless transitions, the second derivative of the ground-state energy is essential for resolving gapless-gapless quantum phase transitions. The combined analysis reveals a rich critical structure arising from the interplay between the transverse magnetic field and ATSI, and underscores the effectiveness of energy-based diagnostics in uncovering quantum critical phenomena.

To gain further insight into the unconventional gapless–gapless transition observed in the system, it is essential to examine quantities that probe correlations and order beyond the excitation spectrum, as such transitions are not associated with the closure of the energy gap but are instead manifested through changes in the underlying ground-state structure and long-range correlations.

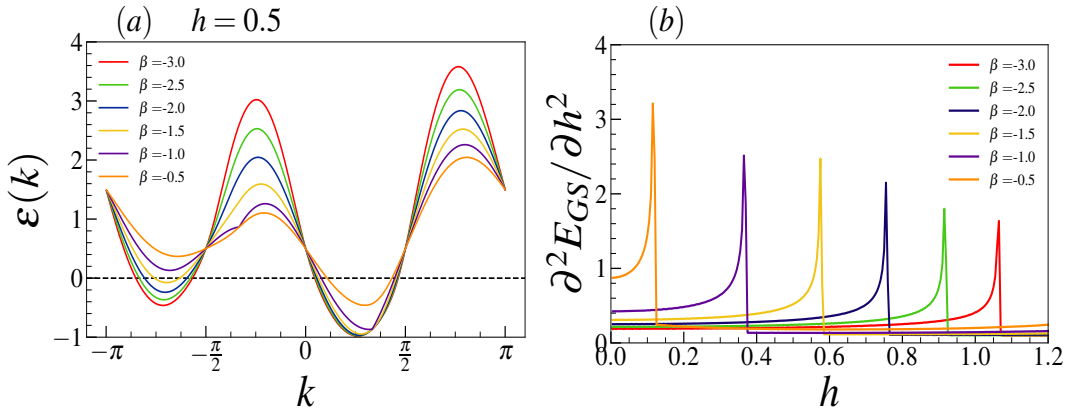


Figure 4. (color online). (a) Dispersion relation $\varepsilon(k)$ as a function of momentum k for $\alpha = 2.0$, $h = 0.5$, and selected anisotropy parameters $\beta = -3, -2.5, -2, -1.5, -1, -0.5$, illustrating the evolution of low-energy states and the Lifshitz transition. (b) Second derivative of the ground-state energy with respect to the magnetic field, $\partial^2 E_G/\partial h^2$, for the same β values, highlighting the nonanalytic features associated with the gapless-gapless transition.

To further elucidate the gapless–gapless transitions identified in the ground-state analysis, we examine the energy spectrum and the corresponding second derivative of the ground-state energy. Figure 4 (a) presents the dispersion relation $\varepsilon(k)$ for a chain of length $N = 1000$, with $\alpha = 2.0$, $h = 0.5$, and selected values of the anisotropy parameter $\beta = -3, -2.5, -2, -1.5, -1, -0.5$. For these values, the energy spectrum intersects the Fermi level at multiple points k, indicating a reconstruction of the low-energy spectrum. Such changes in the number of Fermi points signal a Lifshitz transition, a gapless–gapless quantum phase transition in which the system remains gapless but undergoes a qualitative change in the topology of its Fermi surface.

Figure 4 (b) shows the second derivative of the ground-state energy with respect to the transverse magnetic field, $\partial^2 E_G/\partial h^2$, for the same β values. In agreement with the spectral analysis, the nonanalytic features in these curves occur within the gapless region and coincide with the Lifshitz transition points identified in Fig. 4 (a). This correspondence confirms that the gapless–gapless transition is not captured by the energy gap alone but is encoded in the reconstruction of the low-energy spectrum and the nonanalyticities of the ground-state energy, highlighting the topological nature of the transition in the presence of ATSI and a transverse magnetic field. This result shows that the gapless–gapless Lifshitz transition provides direct information about the reconstruction of the low-energy spectrum rather than in the energy gap itself.

3.2 Magnetization

To gain further insight into the quantum phases and critical behavior of the system, it is useful to examine quantities that capture collective spin order. In particular, the magnetization serves as a natural order parameter for spin-1/2 chains under a transverse magnetic field, providing a direct measure of the alignment of spins along the field direction. It is defined as

$$M^z = \frac{1}{N}\sum_{n=1}^{N}\langle S_n^z\rangle = \frac{1}{N}\sum_{k\in\Lambda}\cos(2\theta_k) + \frac{1}{N}\sum_{k}\sin^2(\theta_k) - \frac{1}{2}. \tag{17}$$

The magnetization reflects the competition between the spin interactions and the external magnetic field. In regions where the field dominates, spins tend to align along its direction, giving rise to a paramagnetic response, while quantum fluctuations can prevent perfect alignment. By analyzing the behavior of M^z across different field strengths and interaction parameters, one can identify the emergence of ordered and disordered phases, locate quantum critical points, and characterize the nature of transitions, including gapless–gapless transitions and gapped phases, within the anisotropic three-spin XX chain.

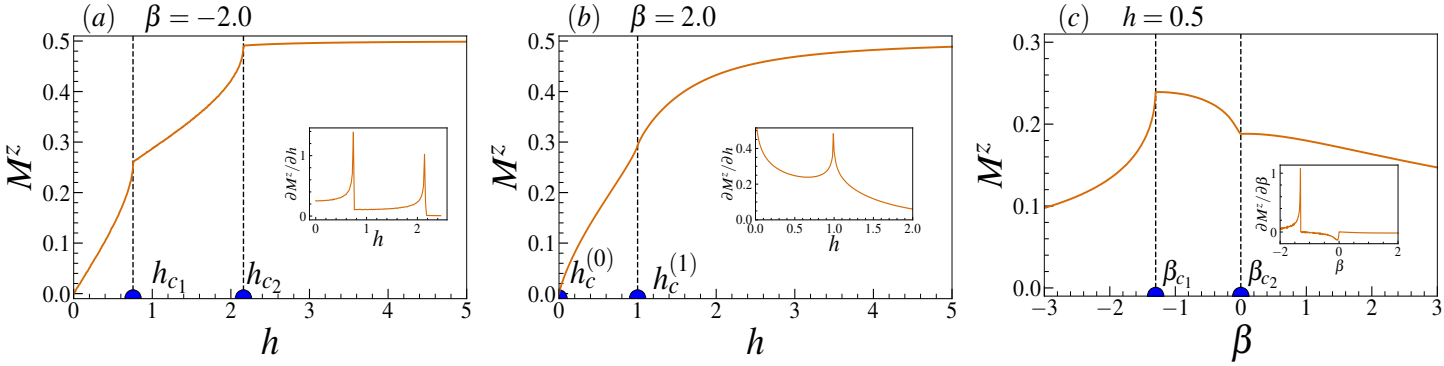


Figure 5. (color online). Magnetization: (a) as functions of h for $\beta = -2.0$, (b) as functions of h for $\beta = 2.0$, (c) as functions of β for $h = 0.5$. All results are obtained for a chain of size $N = 1000$ and $\alpha = 2.0$.

Figure 5 presents the magnetization M^z and its first derivative for the spin-1/2 XX chain with ATSI, highlighting field- and interaction-driven quantum phase transitions. All results are obtained for a chain of size $N = 1000$ with $\alpha = 2.0$.

For $\beta \neq -1$, the magnetization is not a conserved quantity. This follows directly from Eq. (3), where the term proportional to $\alpha(\beta+1)$ represents fermion-pair creation and annihilation and therefore does not conserve the total fermion number, or equivalently the magnetization. Consequently, the ground state is not restricted to a fixed magnetization sector, and the magnetization generally does not reach the fully polarized value $M^z = 0.5$ at any finite field. Instead, it approaches this value asymptotically as $h \to \infty$. The special case $\beta = -1$ is distinguished by the vanishing of the pairing term, for which the magnetization is conserved.

In Fig. 5 (a), the magnetization is plotted as a function of the transverse magnetic field for $\beta = -2.0$. The magnetization increases immediately with the applied field and rises rapidly until h_{c_1}, after which it continues to increase with a lower slope. The inset shows the first derivative of the magnetization, exhibiting two clear peaks that signal these transitions. Since $\beta = -2 \neq -1$, the magnetization does not reach the fully saturated value $M^z = 0.5$ at h_{c_2}; instead, it approaches this value only asymptotically at sufficiently large fields. Thus, h_{c_2} should not be interpreted as a saturation field, but rather as the gapless–gapped quantum phase transition identified from the excitation spectrum. The behavior around h_{c_1} demonstrates that the system undergoes a change in its spin response at the gapless–gapless Lifshitz transition, which is not accompanied by the opening of an excitation gap. The nonanalytic behavior of the magnetization derivative therefore provides a complementary signature of both critical fields.

Figure 5 (b) shows the magnetization for $\beta = 2.0$ as a function of the field. Here, the derivative exhibits a single peak at $h_c^{(1)} = 1.0$, marking the field-driven quantum phase transition. The magnetization remains below the fully polarized value $M^z = 0.5$ at finite fields, reflecting the non-conservation of magnetization and the quantum fluctuations induced by the anisotropic three-spin interaction. It approaches the fully polarized value only asymptotically as h increases. Consistent with previous studies[24], this partial alignment of spins indicates a partially aligned spin-ordered phase, where the spins exhibit a nontrivial correlation structure under the influence of the magnetic field.

In Fig. 5 (c), the magnetization is plotted as a function of β for a fixed field $h = 0.5$. For $\beta < 0$, the derivative identifies a transition within the gapless region, corresponding to the gapless–gapless Lifshitz-type transition identified in the energy

spectrum. The nonanalytic behavior of the derivative reveals changes in the spin response even in the absence of a gap opening, highlighting the restructuring of the low-energy excitations across the Lifshitz transition.
Overall, these results demonstrate that magnetization and its derivative provide a sensitive probe of quantum criticality. They capture both conventional gapless–gapped transitions and subtle gapless–gapless transitions driven by the interplay between the transverse magnetic field and the anisotropic three-spin interactions, reflecting the rich and complex structure of the ground-state phase diagram. For $\beta \neq -1$, these magnetization features should be understood as changes in the ground-state response rather than changes between fixed-magnetization sectors, owing to the non-conservation of magnetization induced by the anisotropic three-spin interaction.

3.3 Cluster order parameters

In quantum many-body systems, order parameters and response functions serve as fundamental indicators that distinguish between different ground-state phases by capturing the underlying types of order. Typically, an order parameter vanishes in disordered phases, reflecting the symmetry of the system, and acquires a finite value in ordered phases, signalling symmetry breaking. Beyond their role in classification, order parameters provide valuable insights into the nature of quantum phase transitions, which may occur continuously (second-order) or discontinuously (first-order). Analysis of order parameters thus enables a deeper understanding of the mechanisms governing the emergence of distinct quantum phases and the structure of the phase diagram.

In the present model, we focus on cluster order parameters, constructed from products of three spin operators, which have proven to be effective probes of exotic quantum phases. While they do not necessarily conform to conventional long-range order definitions, these parameters capture localized spin correlations and emergent phenomena that arise from cluster spin interactions. For the spin-1/2 chain considered here, the cluster order parameters are defined as[46]:

$$
\begin{aligned}
Cl^{-} &= \frac{1}{N}\sum_{n=1}^{N}\langle (S_n^x S_{n+2}^y - S_n^y S_{n+2}^x) S_{n+1}^z \rangle = -\frac{1}{2N}\sum_{k\in\Lambda}\sin(2k), \\
Cl^{+} &= \frac{1}{N}\sum_{n=1}^{N}\langle (S_n^x S_{n+2}^y + S_n^y S_{n+2}^x) S_{n+1}^z \rangle = \frac{1}{4N}\sum_{k\in\Lambda}\sin(2k)\sin(2\theta_k) - \frac{1}{4N}\sum_{k\notin\Lambda}\sin(2k)\sin(2\theta_k).
\end{aligned}
\tag{18}
$$

These parameters explicitly involve correlations beyond nearest neighbors and can be interpreted as connected correlators:

$$
\begin{aligned}
S_n^x S_{n+2}^y S_{n+1}^z &\propto (S_n^x S_{n+1}^y)(S_{n+1}^x S_{n+2}^y), \\
S_n^y S_{n+2}^x S_{n+1}^z &\propto (S_n^y S_{n+1}^x)(S_{n+1}^y S_{n+2}^x),
\end{aligned}
\tag{19}
$$

highlighting the extended nature of correlations captured by these cluster parameters.

From a symmetry perspective, both Cl^{-} and Cl^{+} break time-reversal symmetry and partially break spin-rotational symmetry. Their key distinction lies in parity: Cl^{-} breaks parity symmetry, whereas Cl^{+} preserves it. The cluster order parameter Cl^{-} is often referred to as the scalar chiral order parameter[58], with a nonzero value indicating the presence of chiral ordering, i.e., a helical arrangement of spins along the chain. Such chiral fluctuations can drive quantum phase transitions between different chiral phases or between chiral and non-chiral phases, without necessarily inducing conventional magnetic order.

On the other hand, Cl^{+} is closely related to spin-nematic order[59–61], which describes a quadrupolar alignment of spins along two perpendicular directions rather than a single axis. However, unlike conventional nematicity, Cl^{+} incorporates mixed spin components that introduce chiral-like correlations, thereby breaking time-reversal symmetry. This hybrid character renders Cl^{+} a chiral-nematic order parameter, reflecting both nematic and chiral correlations. As such, Cl^{+} provides a more general measure of order in spin chains, capturing emergent correlations that conventional nematic parameters cannot fully describe.

Together, Cl^{-} and Cl^{+} serve as complementary order parameters that characterize the rich landscape of gapless and chiral-nematic phases in the present spin-1/2 XX chain with anisotropic three-spin interactions, offering detailed insights into the symmetry-breaking mechanisms and quantum correlations underlying these exotic phases.

Figure 6 presents the behavior of the cluster order parameters Cl^{-} and Cl^{+} under variations of the magnetic field and the three-spin interaction strength, for a chain of size $N = 1000$ and $\alpha = 2.0$. These quantities provide complementary insight into chiral and chiral-nematic ordering across the different quantum phases of the system.

We first examine the field dependence for $\beta = -2.0$. As shown in Fig. 6 (a), the chiral order parameter Cl^{-} attains a finite negative value at low magnetic fields, indicating the presence of a chiral gapless phase characterized by broken parity and time-reversal symmetries. With increasing field strength, Cl^{-} increases in magnitude until the first critical field h_{c_1}, where a noticeable change occurs. The discontinuity in the chiral order parameter at h_{c_1}, marked by a change in its slope, signals a fundamental shift in the ground state. This distinct behavior allows us to classify the phases on either side of the critical point as two separate chiral phases, which we designate as chiral-I (for $h < h_{c_1}$) and chiral-II (for $h_{c_1} < h < h_{c_2}$). Beyond this

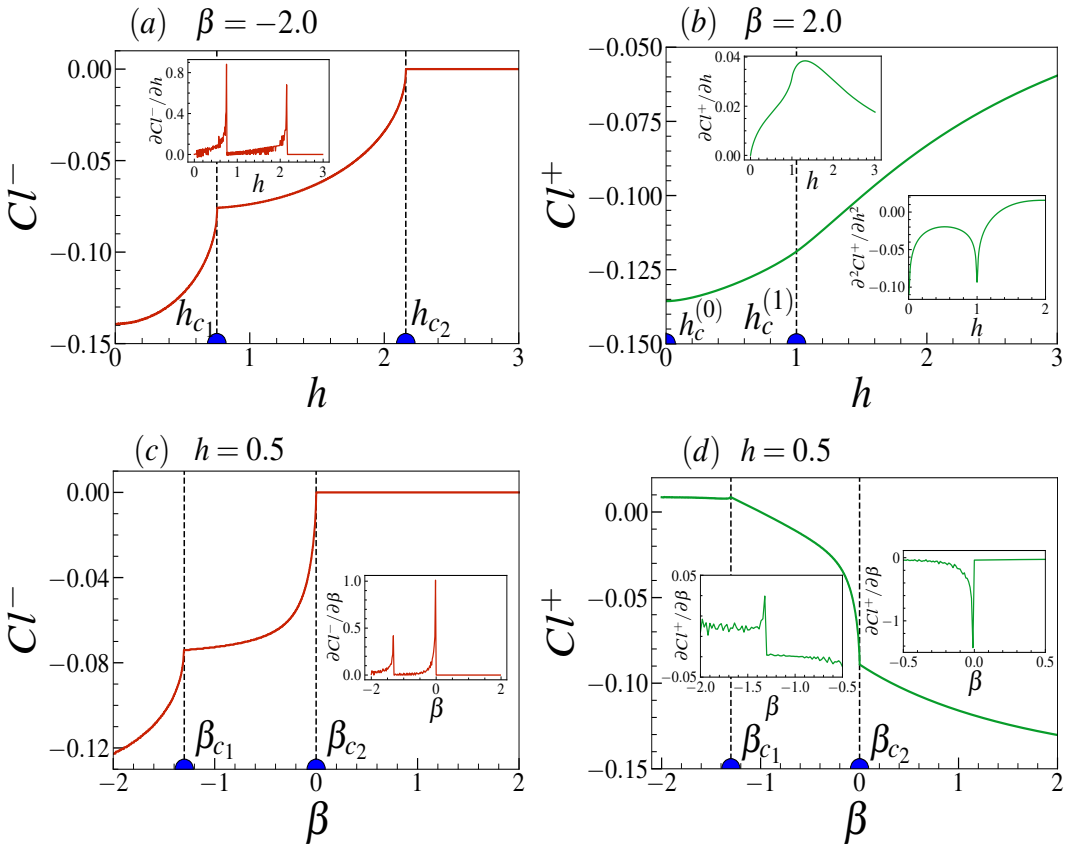


Figure 6. (color online). Left (right) panels show the cluster order parameters Cl^- (Cl^+). (a) Cl^- as functions of the magnetic field h for $\beta = -2.0$. (b) Cl^+ vas functions of the magnetic field h for $\beta = 2.0$. (c,d) $Cl^{\mp}$ as functions of β at fixed $h = 0.5$. All results are obtained for a chain of size $N = 1000$ and $\alpha = 2.0$.

point, Cl^- evolves continuously and eventually vanishes at a second critical field h_{c_2}, signaling a transition into a classical paramagnetic phase. The inset of Fig. 6 (a), displaying the first derivative $\partial Cl^-/\partial h$, exhibits two clear peaks at h_{c_1} and h_{c_2}, clearly identifying the two successive quantum phase transitions. It is also worth noting that the chiral-nematic order parameter Cl^+ remains essentially zero throughout the entire field range for $\beta < 0$.

For $\beta = 2.0$, a qualitatively different scenario emerges. In this regime ($\beta > 0$), the chiral order parameter Cl^- remains zero over the entire magnetic-field range. By contrast, Fig. 6 (b) shows that Cl^+ is finite at low fields and increases smoothly with increasing field strength, approaching but never fully vanishing. Notably, the first derivative $\partial Cl^+/\partial h$ does not exhibit any discontinuity at the critical field $h_c = 1.0$. However, the second derivative displays a clear peak precisely at this field value. This behavior indicates that, while the transition is clearly manifested in conventional thermodynamic quantities, the chiral–nematic order parameter responds more subtly, with criticality appearing only at the level of higher-order derivatives. Such behavior has been observed in related spin systems and reflects the nontrivial nature of the underlying quantum phase transition[24].

The dependence of the cluster order parameters on β at fixed magnetic field $h = 0.5$ is shown in Figs. 6 (c) and 6 (d). As seen in Fig. 6 (c), Cl^- is finite for sufficiently negative values of β, indicating a chiral gapless phase. As β increases, Cl^- grows until the first critical point β_{c_1}, after which it decreases continuously and vanishes at the second critical point $\beta_{c_2} = 0$. Beyond this point, chiral ordering is absent. The inset of Fig. 6 (e), showing $\partial Cl^-/\partial\beta$, confirms these transitions through two well-defined peaks.

Figure 6 (d) displays the behavior of Cl^+ as a function of β for the same parameters. In the region $\beta < \beta_{c_1}$, Cl^+ remains zero, reflecting the absence of chiral–nematic correlations. Upon crossing β_{c_1}, Cl^+ becomes finite and increases rapidly in amplitude, reaching the second transition point at $\beta_{c_2} = 0$. For $\beta > 0.0$, Cl^+ continues to increase smoothly, signaling the stabilization of a chiral–nematic phase. The inset shows the first derivative $\partial Cl^+/\partial\beta$, where two peaks indicate the corresponding critical points.

Taken together, these results establish Cl^- as a robust order parameter for detecting chiral phases, while Cl^+ characterizes the emergence of chiral-nematic ordering in complementary regions of the phase diagram. Importantly, several of the transitions

identified here occur entirely within gapless phases, highlighting that changes in the structure of low-energy correlations, rather than gap opening alone, play a central role in determining the quantum critical behavior of the system.

3.4 Quantum correlation

Quantum correlations play a central role in the characterization of interacting many-body quantum systems, as they encode intrinsically non-classical features that cannot be captured by classical correlations alone[8,62]. In low-dimensional quantum spin systems, such correlations provide particularly powerful insights into exotic phases of matter and quantum critical behavior. Unlike conventional order parameters tied to symmetry breaking, quantum correlations can persist across gapless regimes and often exhibit enhanced sensitivity at quantum phase transitions. As a result, they offer a complementary framework for quantum classification, especially in systems dominated by strong quantum fluctuations.

In this work, we employ two widely used measures of quantum correlations, the concurrence and the QD, to further elucidate the nature of the phases identified through magnetization and order-parameter analyses. Concurrence quantifies bipartite entanglement and captures purely quantum correlations between two spins[63], while QD provides a more general measure that also detects nonclassical correlations present in separable mixed states[64,65]. The combined analysis of these quantities allows us to distinguish between regimes dominated by strong entanglement and those where more general quantum correlations dominate.

The concurrence between two spin-$1/2$ particles located at sites n and m is defined in terms of the two-site reduced density matrix $\rho_{n,m}$, obtained by tracing out all other degrees of freedom. In the standard basis $\{|\uparrow\uparrow\rangle, |\uparrow\downarrow\rangle, |\downarrow\uparrow\rangle, |\downarrow\downarrow\rangle\}$, the reduced density matrix can be written as

$$\rho_{n,m} = \begin{pmatrix} \langle p_n^{\uparrow} p_m^{\uparrow}\rangle & \langle p_n^{\uparrow} S_m^{-}\rangle & \langle S_n^{-} p_m^{\uparrow}\rangle & \langle S_n^{-} S_m^{-}\rangle \\ \langle p_n^{\uparrow} S_m^{+}\rangle & \langle p_n^{\uparrow} p_m^{\downarrow}\rangle & \langle S_n^{-} S_m^{+}\rangle & \langle S_n^{-} p_m^{\downarrow}\rangle \\ \langle S_n^{+} p_m^{\uparrow}\rangle & \langle S_n^{+} S_m^{-}\rangle & \langle p_n^{\downarrow} p_m^{\uparrow}\rangle & \langle p_n^{\downarrow} S_m^{-}\rangle \\ \langle S_n^{+} S_m^{+}\rangle & \langle S_n^{+} p_m^{\downarrow}\rangle & \langle p_n^{\downarrow} S_m^{+}\rangle & \langle p_n^{\downarrow} p_m^{\downarrow}\rangle \end{pmatrix}, \tag{20}$$

where $p^{\uparrow,\downarrow} = \frac{1}{2} \pm \langle S^z\rangle$ and $S^{\pm} = S^x \pm iS^y$. The concurrence is defined as

$$C_{n,m} = \max\left(0, \lambda_1 - \lambda_2 - \lambda_3 - \lambda_4\right), \tag{21}$$

where λ_i are the square roots of the eigenvalues of the matrix $R = \rho_{n,m}\tilde{\rho}_{n,m}$, with $\tilde{\rho}_{n,m} = (\sigma^y \otimes \sigma^y)\rho^*_{n,m}(\sigma^y \otimes \sigma^y)$ denoting the spin-flipped density matrix. Owing to translational invariance and discrete symmetries of the Hamiltonian, the reduced density matrix assumes an X-state structure,

$$\rho_{n,m} = \begin{pmatrix} X^+_{n,m} & 0 & 0 & F^*_{n,m} \\ 0 & Y^+_{n,m} & Z^*_{n,m} & 0 \\ 0 & Z_{n,m} & Y^-_{n,m} & 0 \\ F_{n,m} & 0 & 0 & X^-_{n,m} \end{pmatrix}, \tag{22}$$

where the nonvanishing matrix elements are expressed in terms of fermionic correlation functions as

$$\begin{aligned} X^+_{n,n+1} &= f_0^2 + |f_1|^2 - |f_2|^2, \\ Y^+_{n,n+1} &= Y^-_{n,n+1} = f_0 - X^+_{n,n+1}, \\ X^-_{n,n+1} &= 1 - 2f_0 + X^+_{n,n+1}, \\ Z_{n,n+1} &= f_2, \\ F_{n,n+1} &= f_1, \end{aligned} \tag{23}$$

where

$$\begin{aligned} f_0 &= \frac{1}{N}\sum_{k\in\Lambda} \cos(2\theta_k) + \frac{1}{N}\sum_k \sin^2(\theta_k), \\ f_1 &= -\frac{i}{N}\sum_{k\in\Lambda} \sin(2\theta_k)\sin(k) - \frac{1}{2N}\sum_k \sin(2\theta_k)e^{-ik}, \\ f_2 &= \frac{1}{N}\sum_{k\in\Lambda} [\cos(2\theta_k)\cos(k) - i\sin(k)] + \frac{1}{N}\sum_k \sin^2(\theta_k)e^{-ik}. \end{aligned} \tag{24}$$

In this form, the concurrence simplifies to

$$C_{n,m} = 2\max\left\{0, C^{(1)}_{n,m}, C^{(2)}_{n,m}\right\}, \tag{25}$$

where

$$\begin{aligned} C^{(1)}_{n,m} &= |Z_{n,m}| - \sqrt{X^{+}_{n,m}X^{-}_{n,m}}, \\ C^{(2)}_{n,m} &= |F_{n,m}| - \sqrt{Y^{+}_{n,m}Y^{-}_{n,m}}. \end{aligned} \tag{26}$$

Although concurrence provides a clear measure of bipartite entanglement, it does not capture all quantum correlations present in a many-body system. To overcome this limitation, we also analyze QD, which quantifies the difference between total correlations and their classical component. QD is defined as

$$QD_{n,m} = \mathscr{I}(\rho_{n,m}) - \mathscr{C}(\rho_{n,m}), \tag{27}$$

where the quantum mutual information is given by

$$\mathscr{I}(\rho_{n,m}) = S(\rho_n) + S(\rho_m) - S(\rho_{n,m}), \tag{28}$$

with $S(\rho) = -\mathrm{Tr}(\rho\log\rho)$ denoting the von Neumann entropy. For the X-state density matrices encountered here, quantum discord can be evaluated analytically using the approach. The eigenvalues of $\rho_{n,m}$ are

$$\begin{aligned} \lambda_{0,1} &= \frac{1}{4}\left[1 + c_3 \pm \sqrt{(c_4+c_5)^2 + (c_1-c_2)^2}\right], \\ \lambda_{2,3} &= \frac{1}{4}\left[1 - c_3 \pm \sqrt{(c_4-c_5)^2 + (c_1+c_2)^2}\right], \end{aligned} \tag{29}$$

where the coefficients c_i are expressed in terms of spin correlation functions as

$$\begin{aligned} &c_1 = 2(Z_{n,m} + F_{n,m}), \quad c_2 = 2(Z_{n,m} - F_{n,m}), \\ &c_3 = X^{+}_{n,m} + X^{-}_{n,m} - Y^{+}_{n,m} - Y^{-}_{n,m}, \\ &c_4 = X^{+}_{n,m} - X^{-}_{n,m} - Y^{+}_{n,m} + Y^{-}_{n,m}, \\ &c_5 = X^{+}_{n,m} - X^{-}_{n,m} + Y^{+}_{n,m} - Y^{-}_{n,m}. \end{aligned} \tag{30}$$

The classical correlation $\mathscr{C}(\rho_{n,m})$ is obtained by maximizing over local projective measurements on one of the spins, yielding a closed-form expression. This analytical tractability, together with its sensitivity to changes in correlation structure, makes QD a powerful complementary probe to concurrence for detecting quantum phase transitions and distinguishing between different gapless and correlated phases.

We employ concurrence and QD, we analyze the model from the perspective of quantum correlation, providing a comprehensive characterization of correlations across its phase diagram. Figure 7 summarizes the behavior of nearest-neighbor concurrence and QD across the phase diagram for $N = 1000$ and $\alpha = 2.0$, providing a complementary perspective on the structure of quantum correlations.

The density plots in Fig. 7 (a) and 7 (b) display concurrence and QD, respectively, as functions of h and β. In the region $\beta < 0$, concurrence clearly resolves an intermediate entangled regime: it vanishes in the first gapless phase, becomes finite upon crossing the gapless-gapless transition line, and is finally suppressed again beyond the gapless-gapped transition boundary. This establishes a well-defined window of bipartite entanglement bounded by the two critical lines. For $\beta > 0$, the entangled region is considerably narrower, indicating that only a limited portion of the phase space supports nonzero concurrence. In contrast, QD remains finite already in the first gapless phase, even where concurrence vanishes, and follows the same overall phase boundaries. This demonstrates that nonclassical correlations persist in regions where pairwise entanglement is completely suppressed, highlighting the greater robustness of discord against quantum fluctuations.

To elucidate these features, we consider representative cuts. For $\beta = -2.0$, which is shown in Figs. 7 (c) and 7 (d), concurrence is zero at low fields, signaling a unentangled gapless regime. At the first critical field h_{c_1}, concurrence becomes finite and reaches a maximum in the intermediate phase. It then decreases and vanishes at the second critical point h_{c_2}, remaining zero in the gapped phase. The first derivative of concurrence exhibits clear nonanalyticities at h_{c_1} and h_{c_2}, consistently identifying both transitions. QD, however, is finite already for $h < h_{c_1}$, increases toward a maximum near h_{c_1}, and subsequently decreases

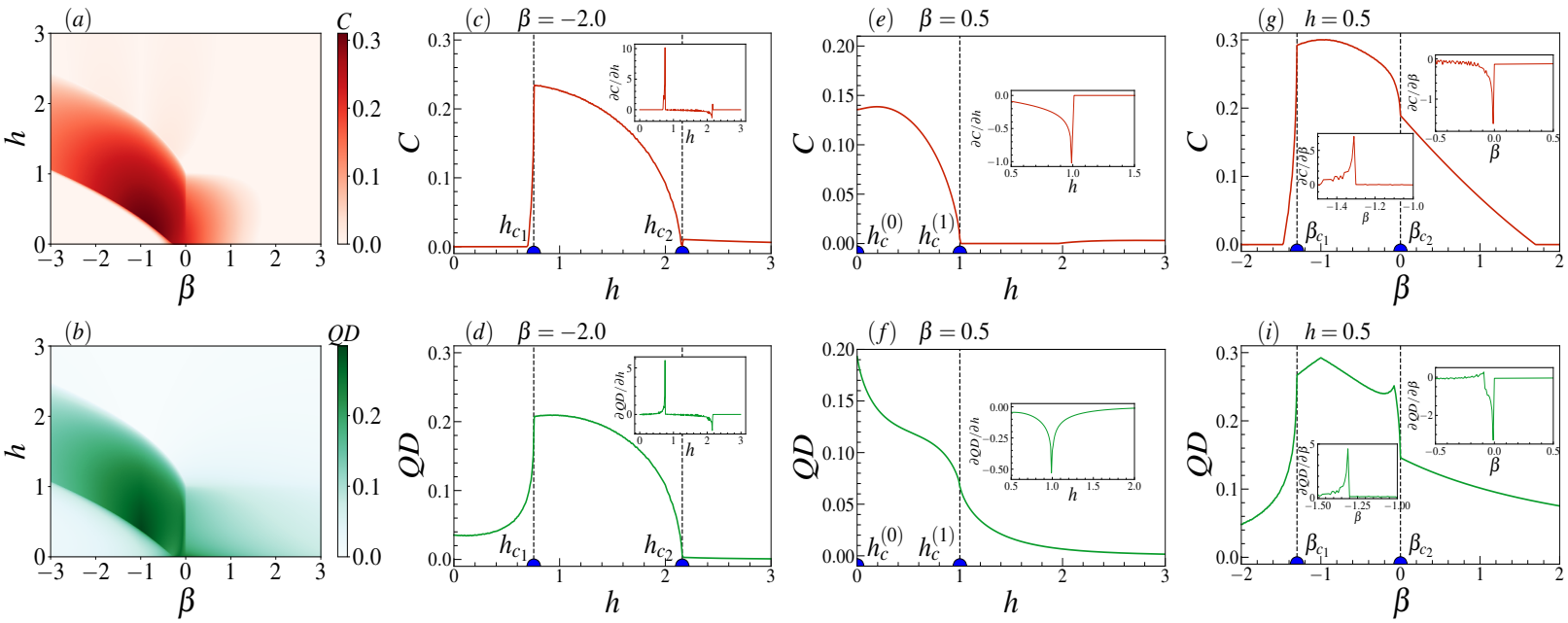


Figure 7. (color online). (a) and (b) Density plots of the nearest-neighbor concurrence and quantum discord (QD), respectively, as functions of the transverse field h and anisotropy β. (c) and (d) Concurrence and QD as functions of h for $\beta = -2.0$. (e) and (f) Concurrence and QD as functions of h for $\beta = 0.5$. (g) and (h) Concurrence and QD as functions of β at fixed $h = 0.5$. All results are obtained for a chain of size $N = 1000$ and $\alpha = 2.0$.

across the second transition, approaching small values in the large-field regime. Its derivative likewise shows clear singular features at both critical fields, confirming that QD faithfully captures the underlying quantum criticality.

For $\beta = 0.5$, as shown in Figs. 7 (e) and 7 (f), where the entangled region is restricted, concurrence decreases with increasing h and vanishes at a single critical point $h_c = 1.0$, beyond which the system remains unentangled. The derivative displays a sharp extremum at h_c, signalling the phase transition. In contrast, QD decreases smoothly with h but remains finite throughout, with its derivative peaking at the same critical field. This again illustrates that discord detects critical behavior even in regimes where entanglement is fragile or absent.

Finally, Figs. 7 (g) and 7 (i) show the dependence on β at fixed field. For $h = 0.5$, concurrence is zero at large values in the $\beta < 0$ regime, becomes finite upon entering the intermediate phase, reaches a maximum near the transition, and decreases toward $\beta = 0$, vanishing at large values in the $\beta > 0$ region. The first derivative signals transitions both within the $\beta < 0$ sector and at $\beta_c = 0$. QD, evaluated at fixed field, remains finite across the entire interval, exhibiting maxima at the transition points and clear nonanalytic behavior in its derivative.

Overall, concurrence identifies a confined entangled sector embedded within the broader phase diagram, while QD reveals that unclassical correlations extend well beyond this region. Both measures display pronounced nonanalyticities at the phase boundaries, demonstrating that entanglement-based correlations provide reliable and sensitive indicators of the gapless–gapless and gapless–gapped quantum phase transitions in the model.

4 Conclusion

In this paper, we have investigated the spin-1/2 XX chain with an anisotropic three-spin interaction under a transverse magnetic field, focusing on the interplay between the anisotropy of the cluster interaction and the external field. By combining the excitation spectrum, ground-state energy, magnetization, cluster order parameters, concurrence, and quantum discord, we have established a unified picture of the field- and anisotropy-driven quantum phases and critical boundaries, as summarized in Fig. 8.

Figure 8 provides a schematic overview of the ground-state phase diagram and summarizes the different quantum phases and transition lines identified throughout this work. In the $\beta < 0$ region, two distinct critical lines are present: a gapless–gapless Lifshitz transition (shown as a red line) and a gapless–gapped second-order transition (shown as a blue line). These lines divide the parameter space into two gapless regimes with qualitatively different correlation properties. For fields below the Lifshitz line, the system resides in a chiral gapless phase characterized by the absence of bipartite entanglement. Upon crossing this line,

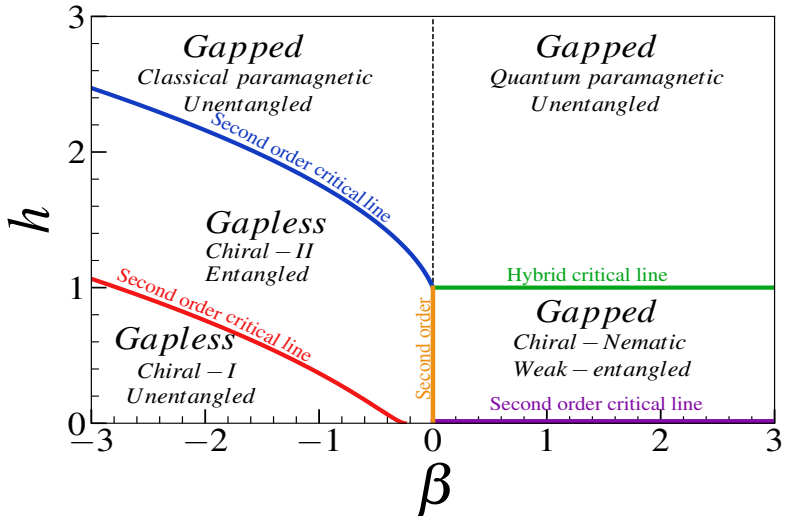


Figure 8. (color online). The ground state phase diagram of the spin-1/2 XX chain model with an anisotropic three-spin interaction in the presence of a transverse magnetic field for $\alpha = 2.0$.

the system enters an intermediate gapless phase where chiral order persists, but finite entanglement develops, before eventually transitioning into a gapped phase beyond the second critical boundary.

In the $\beta > 0$ region, the phase structure contains two field-driven critical boundaries, at $h_c^{(0)} = 0$ and $h_c^{(1)} = 1$. At zero field, the system is gapless, and an infinitesimal transverse field opens a finite gap, defining the $h_c^{(0)} = 0$ critical boundary. At $h_c^{(1)} = 1$, the excitation gap closes and reopens, separating two distinct gapped regimes. Below this line, the system exhibits a gapped chiral-nematic phase with weak but finite entanglement, whereas above it the system remains gapped and enters a regime in which bipartite entanglement is suppressed. This structure demonstrates that the field does not merely drive conventional gap-closing transitions, but can qualitatively reorganize the correlation structure of the anisotropic cluster system.

For $h < 1.0$, the line $\beta_c = 0.0$ defines a second-order quantum phase transition separating the gapless chiral phase in the $\beta < 0.0$ region from the gapped chiral-nematic phase in the $\beta > 0.0$ region. This boundary highlights the qualitative change in both spectral and correlation properties of the ground state induced by the sign of the anisotropic three-spin interaction.

A central outcome of this work is that the anisotropic three-spin interaction provides a richer setting than the corresponding special cases of cluster interactions by allowing the field response to be controlled simultaneously by the anisotropy parameter β and the transverse field. In particular, the $\beta \neq -1$ regime reveals a field-induced reconstruction of the low-energy excitation structure that gives rise to a Lifshitz-type transition between two gapless phases. This transition is accompanied by changes in the number and topology of low-energy Fermi points and by nonanalytic behavior in ground-state and correlation observables, while the excitation gap remains zero. The anisotropic interaction therefore provides a direct route to distinguishing changes in the structure of gapless phases from conventional transitions into gapped phases.

The cluster order parameters Cl^- and Cl^+ further demonstrate that the different regions of the phase diagram are associated with distinct chiral and chiral-nematic correlation patterns. In particular, Cl^- characterizes the chiral sector and its associated symmetry breaking, whereas Cl^+ captures the chiral-nematic correlations in the $\beta > 0$ regime. These results show that the anisotropy of the three-spin interaction is not merely a quantitative modification of the isotropic model, but changes the organization of the ground-state phases and their response to the transverse field.

From a quantum-information perspective, concurrence and quantum discord provide complementary information about the evolution of correlations across the phase diagram. Concurrence identifies a well-defined intermediate entangled regime, while quantum discord remains finite in regions where bipartite entanglement is absent. Their nonanalytic behavior consistently follows the critical boundaries, demonstrating that quantum correlations contain information about the restructuring of the ground state that is not fully captured by conventional order parameters alone.

Taken together, our results demonstrate that the anisotropic three-spin XX chain provides a versatile exactly solvable framework for studying the interplay of cluster interactions, external fields, symmetry-breaking correlations, and unconventional quantum criticality. Beyond identifying the phase boundaries, the present analysis clarifies how anisotropy controls the emergence of distinct gapless and gapped regimes and, in particular, how a field can induce a topological reconstruction of gapless excitations without opening a gap. This establishes the anisotropic cluster interaction as an important extension of previously studied three-spin XX-chain models and provides a useful setting for further investigations of unconventional

quantum phases and quantum correlations in low-dimensional systems.

Author contributions

M.A. and S.M. developed the theoretical framework and methodology. M.A. and N.M. performed the analytical calculations and numerical analysis. M.A. prepared the figures and analyzed the results. M.A., N.M., and S.M. interpreted the results and discussed the physical implications. M.A. wrote the initial draft of the manuscript. All authors reviewed and commented on the manuscript and approved the final version.

Competing interests

The authors declare no competing interests.

Data availability

The data sets used and/or analyzed during the current study are available from the corresponding author upon reasonable request

Funding

This research received no specific grant from any funding agency in the public, commercial, or not-for-profit sectors.

References

1. S. L. Sondhi, S. Girvin, J. Carini, and D. Shahar, "Continuous quantum phase transitions," *Reviews of modern physics*, vol. 69, no. 1, p. 315, 1997.
2. S. Sachdev and B. Keimer, "Quantum criticality," *Physics Today*, vol. 64, no. 2, pp. 29–35, 2011.
3. M. Vojta, "Quantum phase transitions," *Reports on Progress in Physics*, vol. 66, no. 12, p. 2069, 2003.
4. S. Sachdev, *Quantum Phase Transitions*. Cambridge University Press, 2011.
5. P. Gegenwart, Q. Si, and F. Steglich, "Quantum criticality in heavy-fermion metals," *nature physics*, vol. 4, no. 3, pp. 186–197, 2008.
6. Q. Si and F. Steglich, "Heavy fermions and quantum phase transitions," *Science*, vol. 329, no. 5996, pp. 1161–1166, 2010.
7. X.-G. Wen, *Quantum field theory of many-body systems: From the origin of sound to an origin of light and electrons*. Oxford university press, 2004.
8. L. Amico, R. Fazio, A. Osterloh, and V. Vedral, "Entanglement in many-body systems," *Reviews of modern physics*, vol. 80, no. 2, pp. 517–576, 2008.
9. T. Giamarchi, *Quantum physics in one dimension*, vol. 121. Clarendon press, 2003.
10. E. Altman, K. R. Brown, G. Carleo, L. D. Carr, E. Demler, C. Chin, B. DeMarco, S. E. Economou, M. A. Eriksson, K.-M. C. Fu, *et al.*, "Quantum simulators: Architectures and opportunities," *PRX quantum*, vol. 2, no. 1, p. 017003, 2021.
11. A. N. Vasiliev, O. S. Volkova, E. A. Zvereva, and M. Markina, *Low-dimensional magnetism*. CRC Press, 2019.
12. A. Vasiliev, O. Volkova, E. Zvereva, and M. Markina, "Milestones of low-d quantum magnetism," *npj Quantum Materials*, vol. 3, no. 1, p. 18, 2018.
13. B. Keimer, S. A. Kivelson, M. R. Norman, S. Uchida, and J. Zaanen, "From quantum matter to high-temperature superconductivity in copper oxides," *Nature*, vol. 518, no. 7538, pp. 179–186, 2015.
14. X.-G. Wen, "Topological orders in rigid states," *International Journal of Modern Physics B*, vol. 4, no. 02, pp. 239–271, 1990.
15. I. Bloch, J. Dalibard, and S. Nascimbene, "Quantum simulations with ultracold quantum gases," *Nature Physics*, vol. 8, no. 4, pp. 267–276, 2012.
16. Z. Cai, R. Babbush, S. C. Benjamin, S. Endo, W. J. Huggins, Y. Li, J. R. McClean, and T. E. O'Brien, "Quantum error mitigation," *Reviews of Modern Physics*, vol. 95, no. 4, p. 045005, 2023.
17. G. Wendin, "Quantum information processing with superconducting circuits: a review," *Reports on Progress in Physics*, vol. 80, no. 10, p. 106001, 2017.

18. M. Hayashi, S. Ishizaka, A. Kawachi, G. Kimura, and T. Ogawa, *Introduction to quantum information science*. Springer, 2014.

19. E. Lieb, T. Schultz, and D. Mattis, "Two soluble models of an antiferromagnetic chain," *Annals of Physics*, vol. 16, no. 3, pp. 407–466, 1961.

20. P. R. Pasnoori, J. Lee, J. Pixley, N. Andrei, and P. Azaria, "Boundary quantum phase transitions in the spin-1 2 heisenberg chain with boundary magnetic fields," *Physical Review B*, vol. 107, no. 22, p. 224412, 2023.

21. M. Abbasi, S. Mahdavifar, and M. Motamedifar, "Concurrenceless and qdless line in the ground state phase diagram of the spin-1/2 xx chain with uniform gamma interaction," *Results in Physics*, p. 108362, 2025.

22. J. Jahangiri, M. Abbasi, and S. Mahdavifar, "Quantum correlations in spin-1/2 xxz chains with modulated magnetic fields and modulated dzyaloshinskii–moriya interaction," *Chinese Journal of Physics*, vol. 83, pp. 73–85, 2023.

23. M. Abbasi, S. Mahdavifar, and M. Motamedifar, "Spin-1/2 xx chains with modulated gamma interaction," *SciPost Physics Core*, vol. 8, no. 1, p. 001, 2025.

24. M. Abbasi, S. Mahdavifar, and M. Motamedifar, "Hybrid critical line in the spin-1/2 xx chain with gamma interaction under transverse fields," *Scientific Reports*, vol. 15, no. 1, p. 20469, 2025.

25. J. C. Budich and E. Ardonne, "Equivalent topological invariants for one-dimensional majorana wires in symmetry class *d*," *Phys. Rev. B*, vol. 88, p. 075419, Aug 2013.

26. F. Pollmann, A. M. Turner, E. Berg, and M. Oshikawa, "Entanglement spectrum of a topological phase in one dimension," *Physical Review B—Condensed Matter and Materials Physics*, vol. 81, no. 6, p. 064439, 2010.

27. N. Laflorencie, "Quantum entanglement in condensed matter systems," *Physics Reports*, vol. 646, pp. 1–59, 2016.

28. F. K. Fumani, H. Cheraghi, and S. Mahdavifar, "Topological phases, quantum criticality, and bulk entanglement in spin-1/2 xx chain with anisotropic three-spin interactions," *Results in Physics*, p. 108506, 2025.

29. S. Mahdavifar and F. K. Fumani, "Topological phases driven by anisotropic four-spin interactions in 1d spin-1/2 xx chains," *Annalen der Physik*, p. e00435, 2025.

30. P. T. Dumitrescu, A. Goremykina, S. A. Parameswaran, M. Serbyn, and R. Vasseur, "Kosterlitz-thouless scaling at many-body localization phase transitions," *Physical Review B*, vol. 99, no. 9, p. 094205, 2019.

31. R. Blatt and C. F. Roos, "Quantum simulations with trapped ions," *Nature Physics*, vol. 8, no. 4, pp. 277–284, 2012.

32. M. Imada, A. Fujimori, and Y. Tokura, "Metal-insulator transitions," *Reviews of modern physics*, vol. 70, no. 4, p. 1039, 1998.

33. R. Jördens, N. Strohmaier, K. Günter, H. Moritz, and T. Esslinger, "A mott insulator of fermionic atoms in an optical lattice," *Nature*, vol. 455, no. 7210, pp. 204–207, 2008.

34. D. Jaksch, C. Bruder, J. I. Cirac, C. W. Gardiner, and P. Zoller, "Cold bosonic atoms in optical lattices," *Physical Review Letters*, vol. 81, no. 15, p. 3108, 1998.

35. I. Bloch, J. Dalibard, and W. Zwerger, "Many-body physics with ultracold gases," *Reviews of modern physics*, vol. 80, no. 3, pp. 885–964, 2008.

36. J. Clarke and F. K. Wilhelm, "Superconducting quantum bits," *Nature*, vol. 453, no. 7198, pp. 1031–1042, 2008.

37. P. Lou, W.-C. Wu, and M.-C. Chang, "Quantum phase transition in spin-1 2 xx heisenberg chain with three-spin interaction," *Physical Review B—Condensed Matter and Materials Physics*, vol. 70, no. 6, p. 064405, 2004.

38. J. K. Pachos and M. B. Plenio, "Three-spin interactions in optical lattices and criticality in cluster hamiltonians," *Physical review letters*, vol. 93, no. 5, p. 056402, 2004.

39. O. Derzhko, T. Krokhmalskii, J. Stolze, and T. Verkholyak, "Deformable spin-1 2 xx chain with three-site interactions at zero and finite temperatures," *Physical Review B—Condensed Matter and Materials Physics*, vol. 79, no. 9, p. 094410, 2009.

40. W. Cheng and J.-M. Liu, "Fidelity susceptibility approach to quantum phase transitions in the xy spin chain with multisite interactions," *Physical Review A—Atomic, Molecular, and Optical Physics*, vol. 82, no. 1, p. 012308, 2010.

41. Y.-C. Li and H.-Q. Lin, "Thermal quantum and classical correlations and entanglement in the xy spin model with three-spin interaction," *Physical Review A—Atomic, Molecular, and Optical Physics*, vol. 83, no. 5, p. 052323, 2011.

42. T. M. Carrijo, A. T. Avelar, and L. C. Céleri, "Quantum uncertainty in critical systems with three spins interaction," *Journal of Physics B: Atomic, Molecular and Optical Physics*, vol. 48, no. 12, p. 125501, 2015.

43. S. Kheiri, S. Kheiri, and S. Mahdavifar, "Dynamical phase transitions and criticality-enhanced charging in a topological quantum battery," *Phys. Rev. Res.*, pp. –, Mar 2026.

44. S. Mahdavifar, F. K. Fumani, and M. Soltani, "Chiral entanglement landscapes: Insights from a four-spin interaction," *Journal of Magnetism and Magnetic Materials*, p. 174158, 2026.

45. F. Khastehdel Fumani, S. Mahdavifar, and K. Afrousheh, "Entangled unique coherent line in the ground-state phase diagram of the spin-1/2 xx chain model with three-spin interaction," *Physical Review E*, vol. 109, no. 4, p. 044142, 2024.

46. N. Mahboob, S. Mahdavifar, and F. Khastehdel Fumani, "Ground state analysis of the spin-1/2 xx chain model with anisotropic three-spin interaction," *SciPost Physics Core*, vol. 8, no. 3, p. 050, 2025.

47. A. Bermudez, D. Porras, and M. Martin-Delgado, "Competing many-body interactions in systems of trapped ions," *Physical Review A—Atomic, Molecular, and Optical Physics*, vol. 79, no. 6, p. 060303, 2009.

48. O. Katz, L. Feng, A. Risinger, C. Monroe, and M. Cetina, "Demonstration of three-and four-body interactions between trapped-ion spins," *Nature Physics*, vol. 19, no. 10, pp. 1452–1458, 2023.

49. B. Andrade, Z. Davoudi, T. Graß, M. Hafezi, G. Pagano, and A. Seif, "Engineering an effective three-spin hamiltonian in trapped-ion systems for applications in quantum simulation," *Quantum Science and Technology*, vol. 7, no. 3, p. 034001, 2022.

50. M. Topilko, T. Krokhmalskii, O. Derzhko, and V. Ohanyan, "Magnetocaloric effect in spin-1/2 xx chains with three-spin interactions," *The European Physical Journal B*, vol. 85, no. 8, p. 278, 2012.

51. P. Thakur and P. Durganandini, "Orbital antiferroelectricity and higher dimensional magnetoelectric order in the spin-1/2 xx chain extended with three-spin interactions," *The European Physical Journal B*, vol. 96, no. 5, p. 51, 2023.

52. S. Mahdavifar, B. Haghdoost, F. Khastehdel Fumani, and M. Soltani, "Exploring quantum coherence, spin squeezing and entanglement in an extended spin-1/2 xx chain: S. mahdavifar et al.," *Quantum Information Processing*, vol. 23, no. 8, p. 284, 2024.

53. V. Subrahmanyam, "Quantum correlations in a cluster spin model with three-spin interactions," *Journal of Physics A: Mathematical and Theoretical*, vol. 58, no. 13, p. 135301, 2025.

54. V. Derzhko, O. Derzhko, and J. Richter, "Exact solution of a spin-1 2 xx chain with three-site interactions in a random transverse field: Influence of randomness on the quantum phase transition," *Physical Review B—Condensed Matter and Materials Physics*, vol. 83, no. 17, p. 174428, 2011.

55. R. K. Malakar and A. K. Ghosh, "Magnetic phases of xy model with three-spin terms: interplay of topology and entanglement," *Journal of Physics: Condensed Matter*, vol. 36, no. 32, p. 325401, 2024.

56. T. Krokhmalskii, O. Derzhko, J. Stolze, and T. Verkholyak, "Dynamic properties of the spin-1 2 xy chain with three-site interactions," *Physical Review B—Condensed Matter and Materials Physics*, vol. 77, no. 17, p. 174404, 2008.

57. M. Mahmoudi, S. Mahdavifar, T. M. A. Zadeh, and M. Soltani, "Non-markovian dynamics in the extended cluster spin-1/2 xx chain," *Physical Review A*, vol. 95, no. 1, p. 012336, 2017.

58. X.-G. Wen, F. Wilczek, and A. Zee, "Chiral spin states and superconductivity," *Physical Review B*, vol. 39, no. 16, p. 11413, 1989.

59. R. Mao, Y.-W. Dai, S. Y. Cho, and H.-Q. Zhou, "Quantum coherence and spin nematic to nematic quantum phase transitions in biquadratic spin-1 and spin-2 xy chains with rhombic single-ion anisotropy," *Physical Review B*, vol. 103, no. 1, p. 014446, 2021.

60. S. Jiang, J. Romhányi, S. R. White, M. Zhitomirsky, and A. Chernyshev, "Where is the quantum spin nematic?," *Physical Review Letters*, vol. 130, no. 11, p. 116701, 2023.

61. K. Penc and A. M. Läuchli, "Spin nematic phases in quantum spin systems," in *Introduction to frustrated magnetism: materials, experiments, theory*, pp. 331–362, Springer, 2010.

62. R. Horodecki, P. Horodecki, M. Horodecki, and K. Horodecki, "Quantum entanglement," *Reviews of modern physics*, vol. 81, no. 2, pp. 865–942, 2009.

63. W. K. Wootters, "Entanglement of formation of an arbitrary state of two qubits," *Physical Review Letters*, vol. 80, no. 10, p. 2245, 1998.

64. H. Ollivier and W. H. Zurek, "Quantum discord: a measure of the quantumness of correlations," *Physical review letters*, vol. 88, no. 1, p. 017901, 2001.

65. M. S. Sarandy, "Classical correlation and quantum discord in critical systems," *Physical Review A—Atomic, Molecular, and Optical Physics*, vol. 80, no. 2, p. 022108, 2009.